Journal of Solid State Chemistry 183 (2010) 1970–1979

Contents lists available at ScienceDirect

Journal of Solid State Chemistry

journal homepage: www.elsevier.com/locate/jssc

A new structure type of $RE_4B_4O_{11}F_2$: High-pressure synthesis and crystal structure of $La_4B_4O_{11}F_2$

Almut Haberer [a], Reinhard Kaindl [b], Oliver Oeckler [c], Hubert Huppertz [a,*]

[a] Institut für Allgemeine, Anorganische und Theoretische Chemie, Leopold-Franzens-Universität Innsbruck, Innrain 52a, A-6020 Innsbruck, Austria
[b] Institut für Mineralogie und Petrographie, Leopold-Franzens-Universität Innsbruck, Innrain 52, A-6020 Innsbruck, Austria
[c] Department Chemie, Ludwig-Maximilians-Universität München, Butenandtstrasse 5–13, D-81377 München, Germany

ARTICLE INFO

Article history:
Received 5 May 2010
Received in revised form
28 June 2010
Accepted 28 June 2010
Available online 7 July 2010

Keywords:
High-pressure
Multianvil
Crystal structure
Fluoride borate

ABSTRACT

The first lanthanum fluoride borate $La_4B_4O_{11}F_2$ was obtained in a Walker-type multianvil apparatus at 6 GPa and 1300 °C. $La_4B_4O_{11}F_2$ crystallizes in the monoclinic space group $P2_1/c$ with the lattice parameters $a=778.1(2)$ pm, $b=3573.3(7)$ pm, $c=765.7(2)$ pm, $\beta=113.92(3)°$ ($Z=8$), and represents a new structure type in the class of compounds with the composition $RE_4B_4O_{11}F_2$. The crystal structure contains BO_4-tetrahedra interconnected with two BO_3-groups *via* common vertices, B_2O_5-pyroborate units, and isolated BO_3-groups. The structure shows a wave-like modulation along the *b*-axis. The crystal structure and properties of $La_4B_4O_{11}F_2$ are discussed and compared to $Gd_4B_4O_{11}F_2$.

1. Introduction

Borates have been extensively examined under high-pressure/high-temperature conditions and a large variety of new compounds could be obtained, for example the rare-earth borates $RE_4B_6O_{15}$ (*RE*=Dy, Ho) [1–3], α-$RE_2B_4O_9$ (*RE*=Sm–Ho) [4–6], β-$RE_2B_4O_9$ (*RE*=Gd [7], Dy [8]), $RE_3B_5O_{12}$ (*RE*=Er–Lu) [9], and $Pr_4B_{10}O_{21}$ [10]. Borates, being glass formers in general, show an increased tendency to crystallize under pressure, which seems to be valid for fluorine-containing borates, too. Before we started our high-pressure/high-temperature research, rare-earth fluoride borates were only represented by the compounds $RE_3(BO_3)_2F_3$ (*RE*=Sm, Eu, Gd) [11,12] and $Gd_2(BO_3)F_3$ [13], synthesized by heating stoichiometric mixtures of RE_2O_3, B_2O_3, and REF_3 under ambient pressure. Recently, the field of rare-earth fluoride borates could be extended with the high-pressure phases $Yb_5(BO_3)_2F_9$ [14], $Pr_4B_3O_{10}F$ [15], $Gd_4B_4O_{11}F_2$ [16], and the ambient pressure phase $Eu_5(BO_3)_3F$ [17].

Concerning structural motifs, the chemistry of rare-earth fluoride borates under high-pressure/high-temperature conditions shows similarities to that of oxoborates in general. Trigonal-planar BO_3-groups as well as BO_4-tetrahedra were identified and the pressure-induced transformation of the former into the latter ones was observed. The motif of edge-sharing tetrahedra could be realized under high pressure for the compounds $RE_4B_6O_{15}$ (*RE*=Dy, Ho) [1–3] and α-$RE_2B_4O_9$ (*RE*=Sm–Ho) [4–6]. Recently, HP-NiB_2O_4 [18] and β-FeB_2O_4 [19] were synthesized, in which each BO_4-tetrahedron shares a common edge with another one. In fluorido and fluoride borates, this structural feature could not be observed till date.

For the composition $RE_4B_4O_{11}F_2$, two different structure types were obtained by high-pressure/high-temperature synthesis. While the recently presented compound $Gd_4B_4O_{11}F_2$ crystallizes in the space group $C2/c$ [16], the new compound $La_4B_4O_{11}F_2$ shows the same atomic composition, but exhibits a completely different crystal structure in the space group $P2_1/c$. In the crystal structure of $Gd_4B_4O_{11}F_2$, there are BO_3-groups and BO_4-tetrahedra, connected *via* common corners. The structural motif consists of two BO_3-groups (Δ) and two BO_4-tetrahedra (□), and can be described with the fundamental building block 2Δ2□:Δ□□Δ (after Burns et al. [20]), which is a novelty in borate chemistry. In $La_4B_4O_{11}F_2$, the building blocks Δ□Δ and ΔΔ are present, along with isolated BO_3-groups. In the following, the synthesis and the structural details of the new compound $La_4B_4O_{11}F_2$ are reported.

2. Experimental section

2.1. Synthesis

The reaction of the oxides La_2O_3 and B_2O_3 with LaF_3 took place under high-pressure/high-temperature conditions of 6 GPa

* Corresponding author.
E-mail address: hubert.huppertz@uibk.ac.at (H. Huppertz).

0022-4596/$ - see front matter © 2010 Elsevier Inc. All rights reserved.
doi:10.1016/j.jssc.2010.06.019

and 1300 °C, leading to the fluoride borate $La_4B_4O_{11}F_2$ (Eq. (1)):

$$5\ La_2O_3 + 6\ B_2O_3 + 2\ LaF_3 \xrightarrow{6\ GPa,\ 1300\ ^\circ C} 3\ La_4B_4O_{11}F_2 \quad (1)$$

A mixture of La_2O_3 (Strem Chemicals, 99.9%), B_2O_3 (Strem Chemicals, 99.9+%), and LaF_3 (Strem Chemicals, 99.9%) at a molar ratio of 5:6:2 (Eq. (1)) was ground and filled into a boron nitride crucible (Henze BNP GmbH, HeBoSint® S100, Kempten, Germany). This crucible was placed into the center of an 14/8-assembly, which was compressed by eight tungsten carbide cubes (TSM-10 Ceratizit, Reutte, Austria). The details of preparing the assembly can be found in Refs. [21–25]. Pressure was applied by a multianvil device based on a Walker-type module and a 1000 ton press (both devices from the company Voggenreiter, Mainleus, Germany). The sample was compressed up to 6 GPa in 3 h, then heated to 1300 °C in 15 min and kept there for 10 min. Afterwards, the sample was cooled down to 800 °C in 10 min, and cooled down to room temperature by switching off the heating. The decompression of the assembly required 9 h. The recovered MgO-octahedron (pressure transmitting medium, Ceramic Substrates & Components Ltd., Newport, Isle of Wight, UK) was broken apart and the sample was carefully separated from the surrounding boron nitride crucible, and colorless, air- and water-resistant crystal platelets of $La_4B_4O_{11}F_2$ were obtained.

2.2. Crystal structure analysis

The sample characterization was performed by powder X-ray diffraction, carried out in transmission geometry on a flat sample of the reaction product, using a STOE STADI P powder diffractometer with Mo$K\alpha_1$ radiation (Ge monochromator, $\lambda = 70.93$ pm). The powder pattern showed reflections of $La_4B_4O_{11}F_2$ as well as of γ-$La(BO_2)_3$ [26] as a by-product of the synthesis. The experimental powder pattern tallies well with the superimposed theoretical patterns of the two compounds simulated from single-crystal data. Indexing the reflections of the lanthanum fluoride borate, we got the lattice parameters $a = 779.6(6)$ pm, $b = 3573.4(17)$ pm, and $c = 765.8(5)$ pm, with $\beta = 113.94(7)^\circ$ and a unit-cell volume of 1949.9(15) Å^3. This confirmed the lattice parameters, taken from the single-crystal X-ray diffraction study (Table 1).

The intensity data of a single crystal of $La_4B_4O_{11}F_2$ were collected at room temperature using a Nonius Kappa-CCD diffractometer with graded multilayer X-ray optics (Mo$K\alpha$ radiation, $\lambda = 71.073$ pm). Semiempirical scaling complemented by a spherical absorption correction [27,28] was applied to the intensity data. All relevant details of the data collection and evaluation are listed in Table 1.

According to the systematic extinctions, the monoclinic space group $P2_1/c$ was derived. Structure solution and parameter refinement (full-matrix least-squares against F^2) were performed using the SHELX–97 software suite [29,30] with anisotropic atomic displacement parameters for all atoms. The residual peaks after the final difference Fourier syntheses (Table 1) are located very close to the lanthanum cations. Fluorine and oxygen atoms are difficult to distinguish by means of electron density and bond lengths. Therefore, an assignment of the atom types was based on the charge distribution calculations with VaList (*vide infra*) and charge neutrality. The positional parameters of the refinements, interatomic distances, and interatomic angles are listed in Tables 2–4. Further information of the crystal structure is available from the Fachinformationszentrum Karlsruhe (crysdata@fiz-karlsruhe.de), D-76344 Eggenstein-Leopoldshafen (Germany), quoting the Registry no. CSD-421688.

Table 1
Crystal data and structure refinement of $La_4B_4O_{11}F_2$.

Empirical formula	$La_4B_4O_{11}F_2$
Molar mass (g mol^{-1})	812.88
Crystal system	Monoclinic
Space group	$P2_1/c$ (No. 14)
Lattice parameters from powder data	
Powder diffractometer	Stoe StadiP
Radiation	Mo$K\alpha_1$ ($\lambda = 70.93$ pm)
a (pm)	779.6(6)
b (pm)	3573.4(17)
c (pm)	765.8(5)
β (deg.)	113.94(7)
Volume (Å^3)	1949.9(15)
Single-crystal diffractometer	Nonius Kappa-CCD
Radiation	Mo$K\alpha$ ($\lambda = 71.073$ pm)
Single-crystal data	
a (pm)	778.1(2)
b (pm)	3573.3(7)
c (pm)	765.7(2)
β (deg.)	113.92(3)
Volume (Å^3)	1946.3(7)
Formula units per cell	$Z = 8$
Temperature (K)	293(2)
Calculated density (g cm^{-3})	5.548
Crystal size (mm^3)	$0.04 \times 0.02 \times 0.02$
Absorption coefficient (mm^{-1})	17.3
F (000)	2832
θ range (deg.)	$3.3 \le \theta \le 45.4$
Range in $h\ k\ l$	$\pm 15,\ \pm 69,\ -14/15$
Total no. reflections	64178
Independent reflections	15796 ($R_{int} = 0.0532$, $R_\sigma = 0.0488$)
Reflections with $I > 2\sigma(I)$	12135
Data/parameters	15796/379
Absorption correction	Semiempirical
Transm. ratio (min/max)	0.667/0.708
Goodness-of-fit (F^2)	1.024
Final R indices ($I > 2\sigma(I)$)	$R1 = 0.0353$
	$wR2 = 0.0650$
R indices (all data)	$R1 = 0.0577$
	$wR2 = 0.0718$
Largest differ. peak, deepest hole (e/Å^{-3})	4.78/−4.38

2.3. Scanning electron microscopy

Scanning electron microscopy was performed on a JEOL JSM-6500F equipped with a field emission gun at an acceleration voltage of 15 kV. The samples were prepared by placing single crystals on adhesive conductive pads and subsequently coating them with a thin conductive carbon film. Each EDX spectrum (Oxford Instruments) was recorded within a limited area on one single crystal, to avoid the influence of possible contaminating phases.

2.4. IR spectroscopy

FTIR-ATR (Attenuated Total Reflection) spectra of the crystals were recorded with a Bruker Vertex 70 FT-IR spectrometer (resolution ~0.5 cm^{-1}), attached to a Hyperion 3000 microscope in a spectral range from 600 to 4000 cm^{-1}. A frustrum shaped germanium ATR-crystal with a tip diameter of 100 μm was pressed on the surface of the crystals with a power of 5 N, which caused them to crush into pieces of μm-size. 64 scans for sample and background were acquired. Beside spectra correction for atmospheric influences, an enhanced ATR-correction [31], using the OPUS 6.5 software, was performed. A mean refraction index of the sample of 1.6 was assumed for the ATR-correction. Background correction and peak fitting followed *via* polynomial and folded Gaussian–Lorentzian functions.

Table 2
Atomic coordinates (all Wyckoff sites 4*e*) and isotropic equivalent displacement parameters (U_{eq}/Å^2) for $La_4B_4O_{11}F_2$ (space group: $P2_1/c$). U_{eq} is defined as one-third of the trace of the orthogonalized U_{ij} tensor.

Atom	*x*	*y*	*z*	U_{eq}
La1	0.48200(2)	0.234243(5)	0.25646(2)	0.00730(3)
La2	0.86556(2)	0.117015(5)	0.89156(2)	0.00820(3)
La3	0.95956(2)	0.227106(5)	0.74423(2)	0.00921(3)
La4	0.85704(2)	0.138323(5)	0.38092(2)	0.00670(3)
La5	0.36110(2)	0.142117(5)	0.87716(2)	0.00756(3)
La6	0.38039(3)	0.098889(6)	0.38476(3)	0.01150(3)
La7	0.50962(2)	0.016079(5)	0.75693(2)	0.00665(3)
La8	0.99082(2)	0.017185(5)	0.23637(2)	0.00719(3)
B1	0.6053(5)	0.1772(2)	0.6157(4)	0.0080(5)
B2	0.1340(5)	0.0636(2)	0.6169(5)	0.0126(6)
B3	0.2228(4)	0.0588(1)	0.9872(5)	0.0082(5)
B4	0.7638(5)	0.0550(2)	0.5326(5)	0.0085(5)
B5	0.1364(5)	0.1721(2)	0.1780(6)	0.0140(6)
B6	0.6731(6)	0.0695(2)	0.1400(7)	0.0191(7)
B7	0.1625(6)	0.2941(2)	0.9853(6)	0.0184(7)
B8	0.7590(6)	0.1990(2)	0.0783(7)	0.0196(8)
O1	0.6413(3)	0.03099(7)	0.1076(3)	0.0091(3)
O2	0.7167(3)	0.16148(7)	0.0277(3)	0.0107(4)
O3	0.2222(3)	0.04418(7)	0.8153(3)	0.0090(3)
O4	0.5641(4)	0.21490(7)	0.5829(3)	0.0128(4)
O5	0.7887(3)	0.16743(7)	0.6471(3)	0.0100(4)
O6	0.1869(3)	0.09572(7)	0.0025(4)	0.0127(4)
O7	0.1214(3)	0.17874(8)	0.5938(4)	0.0163(5)
O8	0.7443(3)	0.09222(7)	0.5613(3)	0.0125(4)
O9	0.1674(3)	0.25725(8)	0.0479(4)	0.0140(4)
O10	0.1014(3)	0.13927(8)	0.2468(3)	0.0132(4)
O11	0.1172(4)	0.17505(8)	0.9898(4)	0.0164(5)
O12	0.8620(4)	0.08154(8)	0.1746(4)	0.0196(5)
O13	0.9324(3)	0.04124(7)	0.5315(3)	0.0119(4)
O14	0.1279(4)	0.10204(8)	0.6182(4)	0.0183(5)
O15	0.2312(3)	0.04787(8)	0.5059(3)	0.0119(4)
O16	0.4851(3)	0.15034(8)	0.6240(3)	0.0134(4)
O17	0.7890(3)	0.22647(7)	0.9714(3)	0.0108(4)
O18	0.2517(3)	0.03512(8)	0.1360(3)	0.0138(4)
O19	0.6161(4)	0.03160(8)	0.5004(3)	0.0155(5)
O20	0.5589(4)	0.09462(8)	0.1704(4)	0.0154(4)
O21	0.1794(4)	0.20327(8)	0.3039(4)	0.0172(5)
O22	0.7885(4)	0.20890(8)	0.2775(5)	0.0244(6)
F1	0.8728(3)	0.03625(7)	0.8853(3)	0.0147(4)
F2	0.5482(3)	0.08495(7)	0.8028(4)	0.0251(5)
F3	0.4851(3)	0.16134(7)	0.2555(3)	0.0175(4)
F4	0.4119(5)	0.28744(8)	0.4254(4)	0.0282(6)

2.5. Raman spectroscopy

Confocal Raman spectra of single crystals were obtained with a HORIBA JOBIN YVON LabRam-HR 800 Raman micro-spectrometer. The sample was excited by the 532 nm emission line of a 30 mW Nd–YAG-laser under an OLYMPUS 100 × objective (N.A. = 0.9). The size and power of the laser spot on the surface were approximately 1 μm and 5 mW. The scattered light was dispersed by a grating with 1800 lines/mm and collected by a 1024 × 256 open electrode CCD detector. The spectral resolution, determined by measuring the Rayleigh line, was about 1.4 cm^{-1}. The polynomial and convoluted Gauss–Lorentz functions were applied for background correction and band fitting. The wavenumber accuracy of about 0.5 cm^{-1} was achieved by adjusting the zero-order position of the grating and regularly checked by a Neon spectral calibration lamp.

3. Results and discussion

3.1. Crystal structure of $La_4B_4O_{11}F_2$

At first glance, the crystal structure of $La_4B_4O_{11}F_2$ is fairly complicated with a large unit cell (1946.3(7) Å^3) and a total of 42 independent atomic positions. A detailed discussion of the structure mainly based on the different borate fundamental building blocks (FBBs) is presented in the following.

$La_4B_4O_{11}F_2$ consists of BO_3-groups (Δ), BO_4-tetrahedra (□), lanthanum cations, and fluoride anions (Fig. 1). The BO_3-groups are either isolated (Δ), connected *via* common corners (ΔΔ), or connected *via* a BO_4-tetrahedron, forming a fundamental building block (FBB) 2Δ□:Δ□Δ, not yet reported by Burns et al. [20].

With 3573.3(7) pm, the *b* lattice parameter of $La_4B_4O_{11}F_2$ is about five times longer than the other cell edges. Looking at the structure along [00$\bar{1}$], a wave-like modulation of the cations and the B–O-polyhedra with a formal wavelength $\lambda = b$ is observed (Fig. 2). In contrast to the well known *Vernier* phases [32–35], no separation into mismatching substructures was found in $La_4B_4O_{11}F_2$. The three discrete fundamental building blocks Δ, ΔΔ, and Δ□Δ are arranged along each wave in a sheet-like manner, as depicted in Fig. 3 (view along [0$\bar{1}$0]), with the "sheets" expanding in the *bc*-plane. Nevertheless, it should be emphasized that $La_4B_4O_{11}F_2$ is not a layered structure, because the FBBs are not interconnected. There is a set of three different FBB arrangements in each wave, as indicated with dashed lines in Fig. 4. Each set is multiplied by inversion centers, twofold screw axes parallel to the *b*-axis, and *c* glide planes perpendicular to *b*. In arrangement 1, there are the building block Δ□Δ and the isolated BO_3-group of B6 (Fig. 5 top). A detailed view of arrangement 2 is given in Fig. 5 (middle), showing B5 and B7 in form of a pyroborate group. Two further isolated BO_3-groups (B1 and B8, Fig. 5 bottom) are found in arrangement 3, where the planes of the BO_3-groups are orthogonally orientated to each other.

In the isolated BO_3-groups, the B–O-distances range from 134.9(5) to 149.0(6) pm (B1, B6, and B8 in Table 3). This is slightly larger than the values typical for threefold-coordinated boron atoms, e.g. in borates with calcite structure ($AlBO_3$ (137.96(4) pm) [36], β-$YbBO_3$ (137.8(4) pm) [37]), but similarly enlarged bond lengths for BO_3-groups are found as well, e.g. in BaB_8O_{13} (153.5 pm) [38]. The reason for the bond stretching in $La_4B_4O_{11}F_2$ lies in the coordination of the oxygen ions. All isolated BO_3-groups are surrounded by seven lanthanum cations, coordinating their oxygen atoms, as displayed in Fig. 6 for the BO_3-group of B8. This leads to a close packing of $La^{3+}O_n$-polyhedra, which involves stretching of the BO_3-groups and thus enlarge the B–O-bond lengths. The strain of the BO_3-groups can also be seen in the interatomic angles, which slightly deviate from the ideal value of 120° (Table 4).

The corner-sharing BO_3-groups of the pyroborate building block ΔΔ show B–O-distances from 139.1(5) to 145.1(5) pm (B5 and B7 in Table 3). Here, the bond lengths between the boron atoms and the connecting oxygen atom are enlarged, resulting in varying interatomic angles (Table 4). This is known from other pyroborate compounds as well, e.g. from $Eu_2B_2O_5$ [39].

The BO_3-groups of the FBB Δ□Δ show regular average bond-lengths of 137.7 and 138.0 pm, and uniform angles of 120° (B3 and B4 in Tables 3 and 4). Inside the BO_4-tetrahedron, the bond lengths range from 137.3(5) to 164.2(5) pm. The boron atom is displaced from the center of the tetrahedron towards the non-bridging oxygen atoms.

There are eight crystallographically independent La^{3+} ions in the structure, which are nine-, ten-, and elevenfold coordinated by oxygen and fluorine (Fig. 7 and Table 3). The average interatomic distances of the ninefold coordinated La–O/F are 254.1, 253.3, and 255.6 pm and thus in the same range as the average La–O distance of ninefold coordinated La^{3+} cations in LaB_5O_9 (261.6 pm [40]). The average La–O distances of tenfold coordinated La^{3+} cations are larger (263.0, 265.1, 261.8, and 272.3 pm) than would be expected from a tenfold coordination. For La2, the tenfold coordination should rather be described as a 9+1 coordination,

Table 3
Interatomic distances (pm) in $La_4B_4O_{11}F_2$, calculated with the single-crystal lattice parameters.

La1–O4a	241.7(2)	La2–O6	241.5(2)	La3–O5	246.3(2)	La4–O10	250.1(2)
La1–O9	245.9(3)	La2–O2	243.6(2)	La3–O9	247.7(3)	La4–O7	250.1(3)
La1–O4b	248.3(2)	La2–O8	247.7(3)	La3–O11	257.5(3)	La4–O14	251.4(3)
La1–O22	249.4(3)	La2–O5	249.0(2)	La3–O17a	257.5(2)	La4–O8	252.5(2)
La1–O17	268.3(3)	La2–O12	252.1(3)	La3–O17b	258.1(2)	La4–O5	252.9(2)
La1–O21	275.6(3)	La2–O10	271.1(3)	La3–O7	266.0(3)	La4–O12	258.1(3)
La1–F4a	248.1(3)	La2–O11	274.0(3)	La3–O9	267.6(3)	La4–O2	260.7(2)
La1–F4b	249.0(2)	La2–O16	307.6(3)	La3–O22	270.9(3)	La4–O22	263.2(3)
La1–F3	260.5(3)	La2–F2	255.2(2)	La3–O4	284.7(3)	La4–O20	271.8(3)
		La2–F1	288.7(2)	La3–O21	294.8(3)	La4–F3	277.9(2)
La5–O16	250.9(2)	La6–O10	246.0(3)	La7–O19a	246.0(3)	La8–O15	241.5(2)
La5–O14	252.2(3)	La6–O16	248.8(3)	La7–O19b	248.6(3)	La8–O12	247.6(3)
La5–O6	256.1(3)	La6–O15	253.1(2)	La7–O18	249.6(3)	La8–O18	252.7(2)
La5–O7	257.3(3)	La6–O20	254.9(2)	La7–O1a	250.4(2)	La8–O1	253.7(2)
La5–O2	262.3(2)	La6–O8	260.7(3)	La7–O15	251.0(3)	La8–O13a	262.4(2)
La5–O11	265.7(3)	La6–O6	269.7(3)	La7–O1b	251.3(2)	La8–O13b	264.8(3)
La5–O20	273.7(3)	La6–O18	287.7(3)	La7–O3	265.0(2)	La8–O3	268.0(2)
La5–F4	255.1(3)	La6–O19	293.5(3)	La7–F2	248.7(3)	La8–F1a	253.8(2)
La5–F2	270.0(3)	La6–O14	314.8(3)	La7–F1	268.7(2)	La8–F1b	255.6(2)
La5–F3	274.4(2)	La6–F3	269.8(2)				
		La6–F2	296.8(3)				
B1–O16	136.0(4)	B2–O14	137.3(5)	B3–O18	136.3(4)	B4–O19	136.1(4)
B1–O4	138.4(4)	B2–O15	146.0(4)	B3–O6	136.3(4)	B4–O8	136.6(4)
B1–O5	139.2(4)	B2–O3	155.5(4)	B3–O3	141.4(4)	B4–O13	140.5(4)
	Ø=137.9	B2–O13	164.2(5)		**Ø=138.0**		**Ø=137.7**
			Ø=150.8				
B5–O10	139.1(5)	B6–O20	134.9(5)	B7–O9	139.6(6)	B8–O17	135.8(5)
B5–O11	139.1(5)	B6–O1	140.0(5)	B7–O7	139.7(5)	B8–O2	139.7(5)
B5–O21	142.1(5)	B6–O12	145.0(5)	B7–O21	145.1(5)	B8–O22	149.0(6)
	Ø=140.1		**Ø=140.0**		**Ø=141.5**		**Ø=141.5**
F1–La8a	253.8(2)	F2–La7	248.7(3)	F3–La1	260.5(3)	F4–La1a	248.1(3)
F1–La8b	255.6(2)	F2–La2	255.2(2)	F3–La6	269.8(2)	F4–La1b	249.0(2)
F1–La7	268.7(2)	F2–La5	270.0(3)	F3–La5	274.4(2)	F4–La5	255.1(3)
F1–La2	288.7(2)	F2–La6	296.8(3)	F3–La4	277.9(2)		

Table 4
Interatomic angles (deg.) in $La_4B_4O_{11}F_2$, calculated with the single-crystal lattice parameters.

O16–B1–O4	125.6(3)	O14–B2–O15	114.7(3)	O18–B3–O6	120.0(3)	O19–B4–O8	119.1(3)
O16–B1–O5	119.4(3)	O14–B2–O3	116.3(3)	O18–B3–O3	119.1(3)	O19–B4–O13	120.4(3)
O4–B1–O5	115.0(3)	O15–B2–O3	105.6(3)	O3–B3–O6	120.9(3)	O13–B4–O8	120.5(3)
	Ø=120.0	O14–B2–O13	117.4(3)		**Ø=120.0**		**Ø=120.0**
		O15–B2–O13	102.5(3)				
		O3–B2–O13	98.2(2)				
			Ø=109.1				
O10–B5–O11	120.8(3)	O20–B6–O1	127.1(4)	O9–B7–O7	115.6(3)	O17–B8–O2	127.2(4)
O10–B5–O21	116.3(3)	O20–B6–O12	117.4(4)	O9–B7–O21	112.9(4)	O17–B8–O22	116.9(4)
O21–B5–O11	122.7(4)	O12–B6–O1	114.7(3)	O21–B7–O7	131.0(4)	O22–B8–O2	115.7(3)
	Ø=119.9		**Ø=119.7**		**Ø=119.8**		**Ø=119.9**
La8a–F1–La8b	99.20(8)	La7–F2–La2	122.0(2)	La1–F3–La6	145.25(9)	La1a–F4–La1b	106.8(2)
La8a–F1–La7	101.43(8)	La7–F2–La5	137.2(2)	La1–F3–La5	104.69(8)	La1a–F4–La5	137.2(2)
La8b–F1–La7	100.92(8)	La2–F2–La5	98.66(9)	La5–F3–La6	98.69(8)	La1b–F4–La5	114.3(1)
La8a–F1–La2	140.53(9)	La7–F2–La6	92.22(9)	La1–F3–La4	107.72(8)		**Ø=119.4**
La8b–F1–La2	104.48(7)	La6–F2–La2	99.62(9)	La4–F3–La6	93.18(8)		
La7–F1–La2	104.46(7)	La5–F2–La6	93.52(8)	La5–F3–La4	99.33(8)		
	Ø=108.5		**Ø=107.2**		**Ø=108.1**		

as the largest La2–ligand distance is 307.6 pm (La2–O16) and thus about 19 pm larger than the second largest (La2–F1). A similar case is found for elevenfold-coordinated La6, better described as a 10+1 coordination; here, a significant cut in the distance histogram can be observed as well (La6–O14: 314.8(3) pm, Table 3).

The fluoride ions in $La_4B_4O_{11}F_2$ are coordinated by either three or four lanthanum ions (Fig. 8). The bond lengths of the fourfold-coordinated fluoride ions range between 248.7(3) and 296.8(3) pm (Table 3), according with the values for similarly coordinated ions in LaF_3 (247.1–307.0 pm) [41]. The average La–F angles are 108.5°, 107.2°, and 108.1° (Table 4), and thus fairly

close to the ideal tetrahedral angle. The bond lengths of the threefold-coordinated fluoride ion with 248.1(3) to 255.1(3) pm are shorter than expected, and the interatomic angles sum up to 119.4.

The calculations of the charge distribution of the atoms in $La_4B_4O_{11}F_2$ *via* bond valence sums (ΣV) with VaList (bond valence calculation and listing) [42] were performed and confirm the formal valence states in the fluoride borate (Table 5). Slight deviations, for example for O22, occur frequently when calculating bond valence sums with the bond-length/bond-strength concept and are evoked by larger-than-average bond lengths of the corresponding atoms.

To assure the atom assignment in the structure, single crystals of our sample were subjected to elemental analysis *via* SEM/EDX experiments. The crystals showed average atomic La:B:O:F compositions (%) of 16:16:53:15. Due to the light weight of boron, measurements have to be taken with caution, but still, these results confirm the presence of all elements and the composition, obtained from the single crystal structure determination (calculated values (%) La:B:O:F: 19.0:19.0:52.5:9.5).

Furthermore, we calculated the Madelung Part of Lattice Energy (MAPLE) [43–45] for $La_4B_4O_{11}F_2$ in order to compare it with the sum of the MAPLE values of the ambient-temperature modification of La_2O_3 [46], LaF_3 [47], and of the high-pressure modification of B_2O_3 (B_2O_3-II) [48]. The additive potential of the MAPLE values allows the calculation of a hypothetical value for $La_4B_4O_{11}F_2$, starting from binary oxides and fluorides. As result, we obtained a value of 70766 kJ/mol in comparison to 71136 kJ/mol (deviation: 0.5%), starting from the binary components [$5/3 \times La_2O_3$ (14234 kJ/mol)+$2 \times B_2O_3$-II (21938 kJ/mol)+$2/3 \times LaF_3$ (5306 kJ/mol)].

3.2. FTIR spectroscopy

In Figs. 9 and 10, the FTIR-ATR spectra of $La_4B_4O_{11}F_2$ are displayed. The wavenumbers of ATR-bands are given in Table 6. In the range between 600 and 1600 cm^{-1}, four main groups of

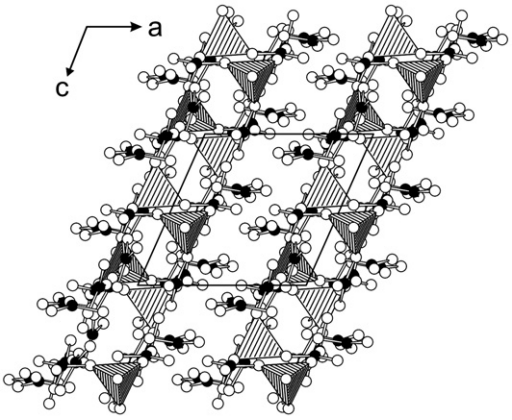

Fig. 3. Sheet-like arrangement of fundamental building blocks in $La_4B_4O_{11}F_2$, viewing along [0$\bar{1}$0].

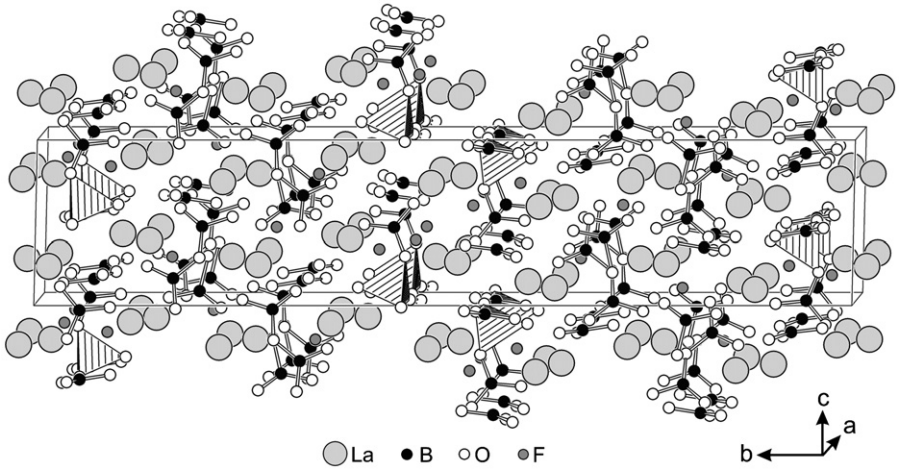

Fig. 1. Crystal structure of $La_4B_4O_{11}F_2$, consisting of La^{3+} and F^- ions, BO_3-groups, and BO_4-tetrahedra.

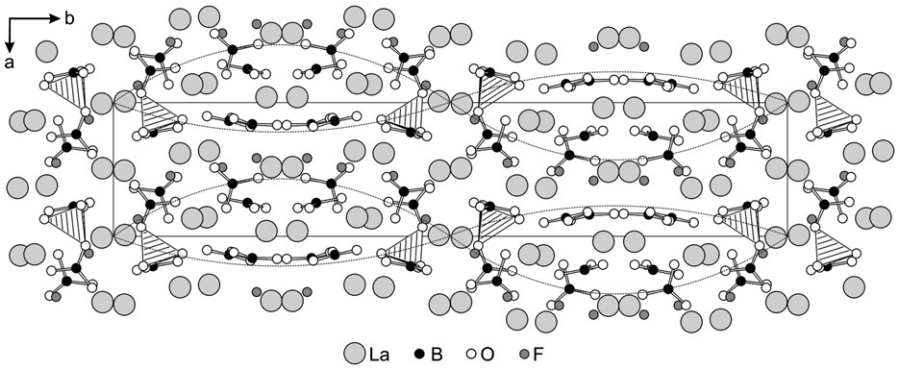

Fig. 2. Wave-like modulations in the crystal structure of $La_4B_4O_{11}F_2$, showing a wavelength of $\lambda = b$.

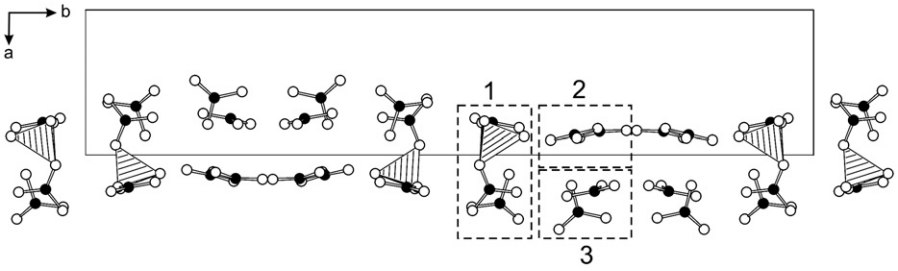

Fig. 4. Location of the FBBs in the crystal structure of $La_4B_4O_{11}F_2$. Each wave is built up from a set of three FBB arrangements (dashed lines).

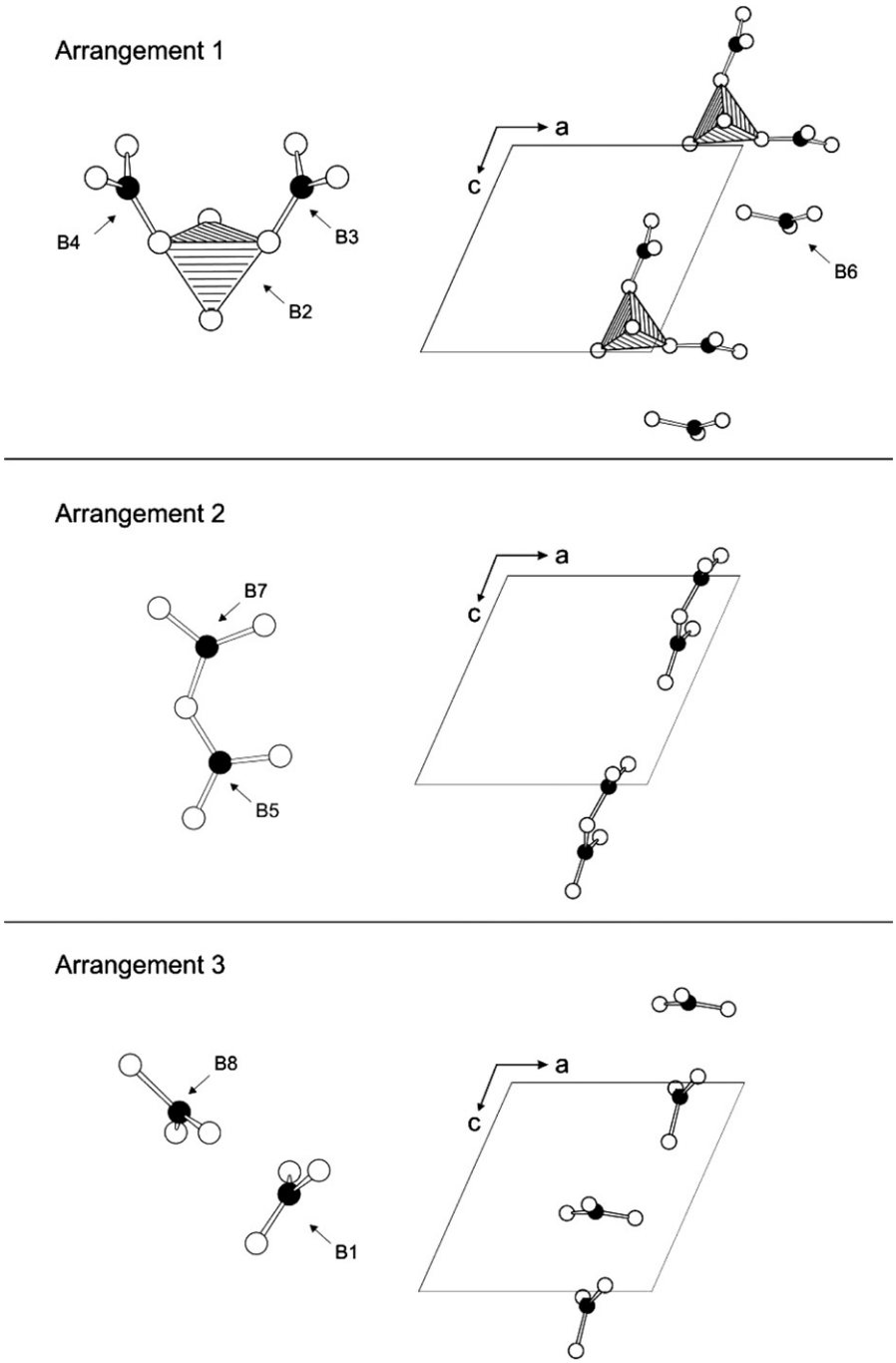

Fig. 5. Detailed view of the FBB arrangements in $La_4B_4O_{11}F_2$. Top: arrangement 1, showing the FBB $\Delta\square\Delta$ (left). Between each FBB, an isolated BO_3-group is positioned (right). Middle: detailed view of arrangement 2, showing the corner-sharing BO_3-groups of the FBB $\Delta\Delta$. Bottom: detailed view of arrangement 3, showing two isolated BO_3-groups in an orthogonal orientation.

bands could be distinguished: bands around 700 cm^{-1} are typical for in-plane and out-of-plane bending vibrations of BO_3-groups; however, in rare-earth metaborates, bands at 725 and 662 cm^{-1} were taken as indication for both three- and fourfold coordinated boron [16,49–51]. Between 900 and 1100 cm^{-1}, stretching vibrations of tetrahedrally coordinated boron atoms are expected. The strong bands in the range of 1200–1500 cm^{-1} are indicative of trigonal borate groups. From 3300 to 3550 cm^{-1}, several weak bands could be detected, suggesting a substitution of trace amounts of hydroxyl groups for fluoride.

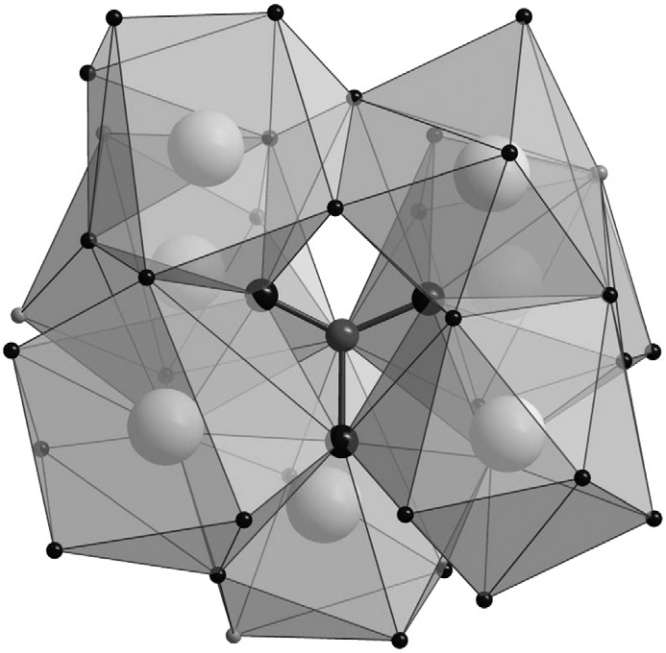

Fig. 6. Surrounding of the isolated BO_3-group (B8) in $La_4B_4O_{11}F_2$.

3.3. Raman spectroscopy

The Raman spectrum and the corresponding wavenumbers of bands of a $La_4B_4O_{11}F_2$ single crystal are displayed in Fig. 11 and Table 7. In total, 40 bands in the range of 100–1600 cm^{-1} could be detected. In contrast to FTIR, no bands were observed between 3000 and 4000 cm^{-1}, which is probably related to the comparatively low sensitivity of Raman spectroscopy for hydroxyl vibrational modes. The Raman spectrum will be compared to the polymorph $Gd_4B_4O_{11}F_2$; the band assignments were made in analogy to structurally and chemically similar borate compounds [5,52–56].

In agreement with the ATR-spectra, the Raman spectrum of $La_4B_4O_{11}F_2$ showed four groups of bands; the three most intense bands occurred around 300 cm^{-1}. In $Gd_4B_4O_{11}F_2$, which contains corner-sharing BO_3-groups and BO_4-tetrahedra, intense bands were observed below 200 cm^{-1} and assigned to cation-oxygen and cation-fluorine bonds, as well as complex lattice vibrations. It has been speculated that these bands are dominantly related to the fluoride ions, which are all fourfold-coordinated by Gd^{3+} ions in $Gd_4B_4O_{11}F_2$. In $La_4B_4O_{11}F_2$, the fluoride ions are both three- and fourfold coordinated and the range of bond lengths (248.7–307.0 pm) is larger than in $Gd_4B_4O_{11}F_2$ (244.8–283.7 pm). This might account for the band differences in this area.

For $La_4B_4O_{11}F_2$, the area of 400–800 cm^{-1} is characterized by 13 weaker bands. The bending and the pulse vibrations of BO_3-groups and BO_4-tetrahedra are expected to be the main vibrational modes contributing to these bands.

Bands between 800 and 1100 cm^{-1} are most frequently assigned to stretching vibrations of the BO_4-tetrahedra. Three intense bands at 825, 916, and 960 cm^{-1} are observed here in contrast to $Gd_4B_4O_{11}F_2$, which shows only one intense band at 959 cm^{-1}. Bands in the range from 1100 to 1600 cm^{-1} are attributed to stretching vibrations of the BO_3-groups. For $La_4B_4O_{11}F_2$, at least 6 intense bands were detected compared to only two for $Gd_4B_4O_{11}F_2$. The most probable explanation for these differences are the different building blocks of the two

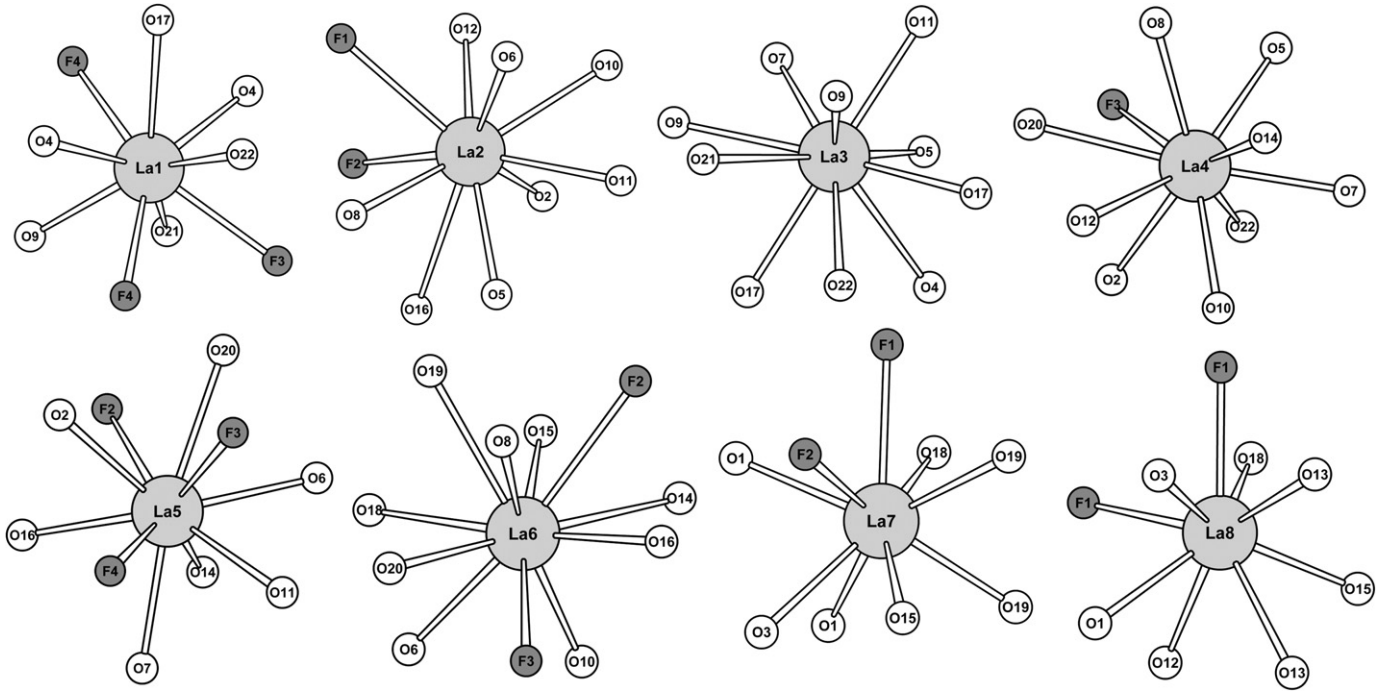

Fig. 7. Coordination spheres of the La^{3+} ions in $La_4B_4O_{11}F_2$.

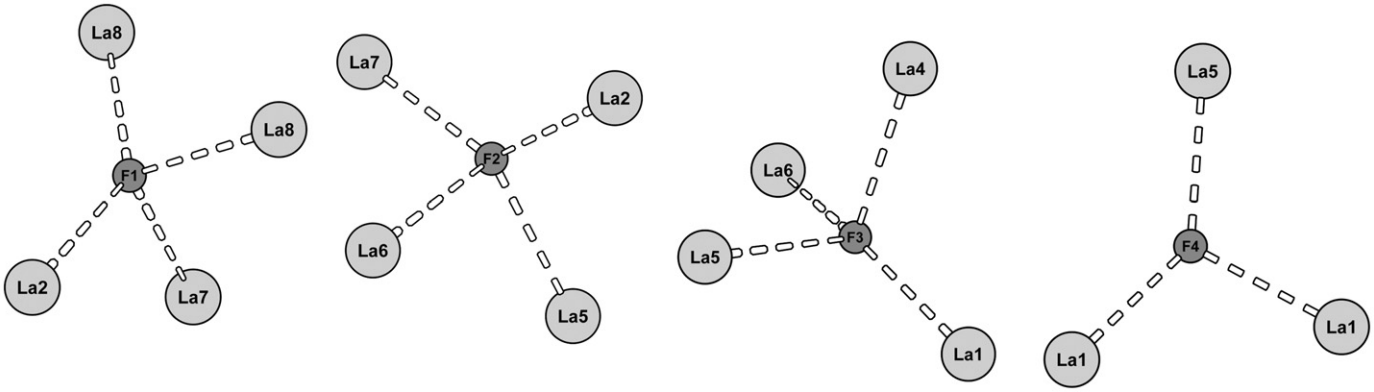

Fig. 8. Coordination of the fluoride ions in $La_4B_4O_{11}F_2$.

Table 5
Bond valence sums (ΣV) in $La_4B_4O_{11}F_2$, calculated with VaList [42].

	La1	La2	La3	La4	La5	La6	La7	La8
ΣV	3.19	3.19	2.94	3.29	2.89	2.80	3.28	3.11
	B1	B2	B3	B4	B5	B6	B7	B8
ΣV	2.94	2.87	2.93	2.95	2.85	2.79	2.67	2.69
	O1	O2	O3	O4	O5	O6	O7	O8
ΣV	2.10	2.03	2.03	2.07	2.20	2.13	1.95	2.15
	O9	O10	O11	O12	O13	O14	O15	O16
ΣV	−2.09	−2.14	−1.77	−1.97	−1.96	−1.81	−2.09	−1.95
	O17	O18	O19	O20	O21	O22		
ΣV	−1.95	−1.97	−2.01	−1.87	−2.01	−1.67		
	F1	F2	F3	F4				
ΣV	−0.87	−0.89	−0.75	−0.95				

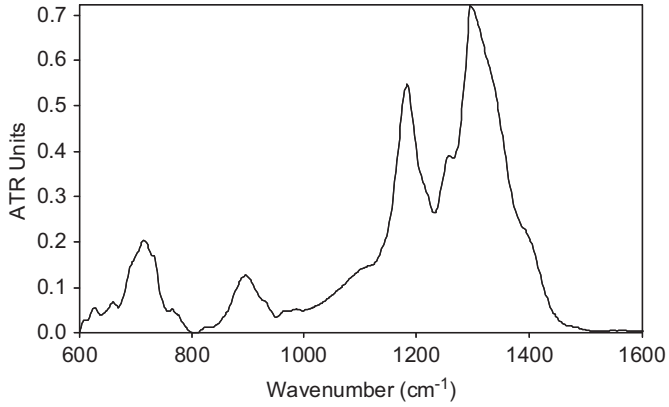

Fig. 9. FTIR-ATR spectrum of $La_4B_4O_{11}F_2$ in the range 600–1600 cm^{-1}.

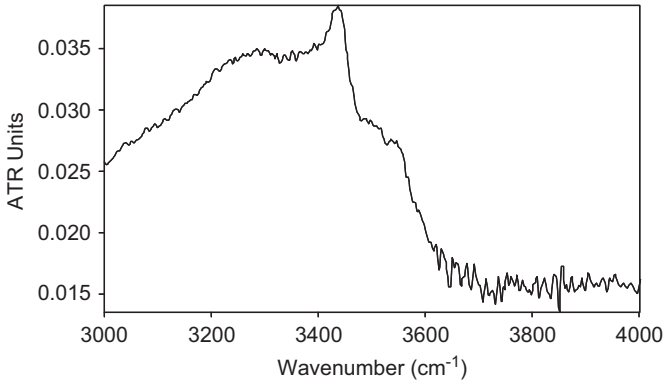

Fig. 10. FTIR-ATR spectrum of $La_4B_4O_{11}F_2$ in the range 3000–4000 cm^{-1}.

compounds and the larger range of B–O bond distances in the BO_3-groups ($La_4B_4O_{11}F_2$:134.9–149.0 pm; $Gd_4B_4O_{11}F_2$:136.1–140.7 pm) and the BO_4-tetrahedra ($La_4B_4O_{11}F_2$: 137.3–164.2 pm; $Gd_4B_4O_{11}F_2$: 141.3–159.0 pm).

4. Conclusions

In this article, we described the high-pressure synthesis and crystal structure of the new lanthanum fluoride borate $La_4B_4O_{11}F_2$. It shows the same composition as the fluoride borate $Gd_4B_4O_{11}F_2$ [16], but exhibits a completely different crystal structure. The structure of $La_4B_4O_{11}F_2$ shows a wave-like modulation along the *b*-axis, generated by the orientation of trigonal BO_3-groups and BO_4-tetrahedra. Elemental analysis confirmed the presence and quantity of fluoride ions in the structure. Single-crystal IR-/Raman spectroscopy complete the structural characterization of the new fluoride borate.

For the future, experiments on the formation range of the compounds $RE_4B_4O_{11}F_2$ shall follow. It will be of great interest to see, which crystal structure is favored by the rare-earth ions of intermediate size and whether it will be possible to obtain both structure types as polymorphs for one and the same cation.

Table 6
Wavenumbers and possible assignment of FTIR-absorption bands in the spectrum of $La_4B_4O_{11}F_2$.

Band	assignment	Band	assignment
629	$\delta(BO_3)$	895	$\nu(BO_4)$
		932	
658	$\delta(BO_3)$, $\delta(BO_4)$	974	
		1093	
		1161	
700	$\delta(BO_3)$	1182	
729	$\delta(BO_3)$, $\delta(BO_4)$	1217	$\nu(BO_3)$
		1253	
		1294	
770	$\delta(BO_3)$	1325	
		1401	
		3302	$\nu(OH)$
		3435	
		3506	
		3548	

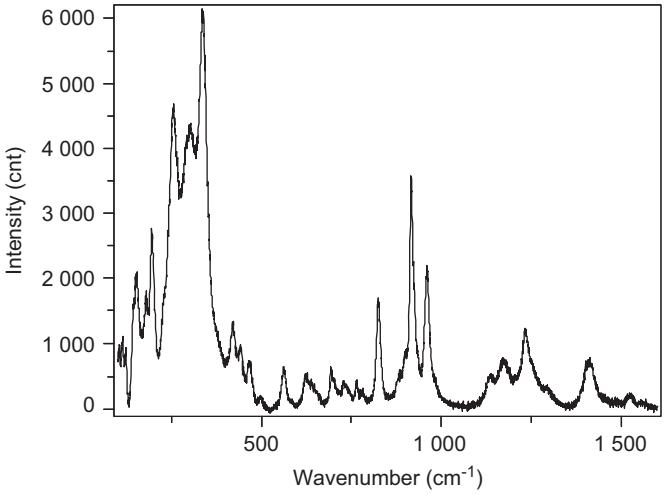

Fig. 11. Raman spectrum of $La_4B_4O_{11}F_2$ in the range 100–1600 cm^{-1}.

Table 7
Wavenumbers and possible assignment of Raman bands in the spectrum of $La_4B_4O_{11}F_2$.

Band	assignment	Band	assignment
104	Lattice	699	bending (BO_4), pulse vibration (BO_3)
115		728	
123		733	
143		764	
153	La–O, F–O	779	
179	bending, stretching $(BO)_3$	825	stretching (BO_4)
197		884	
228		899	
254		916	
299		923	
338		960	
373		973	
421	bending (BO_4), pulse vibration (BO_3)	1134	stretching (BO_3)
442		1173	
467		1233	
497		1257	
562		1297	
622		1411	
637		1494	
692		1525	

Acknowledgments

We thank Dr. Gunter Heymann and Dr. Peter Mayer (LMU München) for collecting the single-crystal data. Special thanks go to Prof. Dr. W. Schnick (LMU München) for his continuous support of these investigations and to Prof. Dr. E. Bertel (LFU Insbruck) for useful discussions.

Appendix A. Supporting Materials

Supplementary data associated with this article can be found in the online version at doi:10.1016/j.jssc.2010.06.019.

References

[1] H. Huppertz, B. von der Eltz, J. Am. Chem. Soc. 124 (2002) 9376.
[2] H. Huppertz, Z. Naturforsch. B 58 (2003) 278.
[3] H. Huppertz, H. Emme, J. Phys.: Condens. Matter 16 (2004) 1283.
[4] H. Emme, H. Huppertz, Z. Anorg. Allg. Chem. 628 (2002) 2165.
[5] H. Emme, H. Huppertz, Chem. Eur. J. 9 (2003) 3623.
[6] H. Emme, H. Huppertz, Acta Crystallogr. C 61 (2005) i29.
[7] H. Emme, H. Huppertz, Acta Crystallogr. C 61 (2005) i23.
[8] H. Huppertz, S. Altmannshofer, G. Heymann, J. Solid State Chem. 170 (2003) 320.
[9] H. Emme, M. Valldor, R. Pöttgen, H. Huppertz, Chem. Mater. 17 (2005) 2707.
[10] A. Haberer, G. Heymann, H. Huppertz, J. Solid State Chem. 180 (2007) 1595.
[11] G. Corbel, R. Retoux, M. Leblanc, J. Solid State Chem. 139 (1998) 52.
[12] E. Antic-Fidancev, G. Corbel, N. Mercier, M. Leblanc, J. Solid State Chem. 153 (2000) 270.
[13] H. Müller-Bunz, Th. Schleid,, Z. Anorg. Allg. Chem. 628 (2002) 2750.
[14] A. Haberer, H. Huppertz, J. Solid State Chem. 182 (2009) 888.
[15] A. Haberer, R. Kaindl, H. Huppertz, Solid State Sci. 12 (2010) 515.
[16] A. Haberer, R. Kaindl, H. Huppertz, J. Solid State Chem. 183 (2010) 471.
[17] K. Kazmierczak, H. A. Höppe, Eur. J. Inorg. Chem. (2010) DOI:10.1002/ejic.201000105.
[18] J. S. Knyrim, F. Roeßner, S. Jakob, D. Johrendt, I. Kinski, R. Glaum, H. Huppertz, Angew. Chem. 119 (2007) 9256; Angew. Chem. Int. Ed. 46 (2007) 9097.
[19] S.C. Neumair, R. Glaum, H. Huppertz, Z. Naturforsch. B 64 (2009) 883.
[20] P.C. Burns, J.D. Grice, F.C. Hawthorne, Can. Mineral. 33 (1995) 1131.
[21] D. Walker, M.A. Carpenter, C.M. Hitch, Am. Mineral. 75 (1990) 1020.
[22] D. Walker, Am. Mineral. 76 (1991) 1092.
[23] H. Huppertz, Z. Kristallogr. 219 (2004) 330.
[24] D.C. Rubie, Phase Transitions 68 (1999) 431.
[25] N. Kawai, S. Endo, Rev. Sci. Instrum. 8 (1970) 1178.
[26] H. Emme, C. Despotopoulou, H. Huppertz, Z. Anorg. Allg. Chem. 630 (2004) 2450.
[27] L.J. Farrugia, J. Appl. Cryst. 32 (1999) 837.
[28] Z. Otwinowski, W. Minor, Methods Enzymol 276 (1997) 307.
[29] G.M. Sheldrick, SHELXS-97 and SHELXL-97, Program suite for the solution and refinement of crystal structures, University of Göttingen, Göttingen, Germany, 1997.
[30] G.M. Sheldrick, Acta Crystallogr. A 64 (2008) 112.
[31] F.M. Mirabella Jr. (ed.), Internal Reflection Spectroscopy, Theory and Applications, Marcel Dekker, Inc. (1992) p. 276.
[32] B.G. Hyde, A.N. Bagshaw, S. Andersson, M. O'Keeffe, Ann. Rev. Mater. Sci. 4 (1974) 43.
[33] D.J.M. Bevan, J. Mohyla, B.F. Hoskins, R.J. Steen, Eur. J. Solid State Inorg. Chem. 27 (1990) 451.
[34] J.P. Laval, A. Taoudi, A. Abaouz, B. Frit, J. Solid State Chem. 119 (1995) 125.
[35] H. Müller-Bunz, O. Janka, Th. Schleid, Z. Anorg. Allg. Chem. 633 (2007) 37.
[36] A. Vegas, Acta Crystallogr. B 33 (1977) 3607.
[37] H. Huppertz, Z. Naturforsch. B 56 (2001) 697.
[38] J. Krogh-Moe, M. Ihara, Acta Crystallogr. B 25 (1969) 2153.
[39] K. Machida, H. Hata, K. Okuno, G. Adachi, J. Shiokawa, J. Inorg. Nucl. Chem. 41 (1979) 1425.
[40] L. Li, X. Jin, G. Li, Y. Wang, F. Liao, G. Yao, J. Lin, Chem. Mater. 15 (2003) 2253.
[41] M. Mansmann, Z. Kristallogr. 122 (1965) 375.
[42] A. S. Wills, VaList Version 3.0.13, University College London, UK, 1998–2008. Program available from www.ccp14.ac.uk.
[43] R. Hoppe, Angew. Chem. 78 (1966) 52; Angew. Chem. Int. Ed. 5 (1966) 96.
[44] R. Hoppe, Angew. Chem. 82 (1970) 7; Angew. Chem. Int. Ed. 9 (1970) 25.
[45] R. Hübenthal, MAPLE - Program for the Calculation of MAPLE Values, Vers. 4, University of Gießen, Gießen, Germany, 1993.
[46] N. Hirosaki, S. Ogata, C. Kocer, J. Alloys Compd. 351 (2003) 31.
[47] E. Staritzky, L.B. Asprey, Anal.Chem. 29 (1957) 856.

[48] C.T. Prewitt, R.D. Shannon, Acta Crystallogr. B 24 (1968) 869.
[49] J.P. Laperches, P. Tarte, Spectrochim. Acta. 22 (1966) 1201.
[50] G. Heymann, K. Beyer, H. Huppertz, Z. Naturforsch. B 59 (2004) 1200.
[51] C.E. Weir, R.A. Schroeder, J. Res. Nat. Bur. Stands 68A (1964) 465.
[52] L. Jun, X. Shuping, G. Shiyang, Spectrochim. Acta A 51 (1995) 519.
[53] G. Chadeyron, M. El-Ghozzi, R. Mahiou, A. Arbus, J.C. Cousseins, J. Solid State Chem. 128 (1997) 261.
[54] H. Huppertz, J. Solid State Chem. 177 (2004) 3700.
[55] C. Zhang, Y.H. Wang, X. Guo, J. Lumin. 122–123 (2007) 980.
[56] G. Padmaja, P. Kistaiah, J. Phys. Chem. A 113 (2009) 2397.